Nanoscale

COMMUNICATION

The facile synthesis of Cu@SiO₂ yolk-shell nanoparticles via the disproportionation reaction of silica-encapsulated Cu₂O nanoparticle aggregates

Jianwei Jiang, Sang-Ho Kim[*], and Longhai Piao[*]

Encapsulation of the nanoparticle (NP) followed by tailoring of the core materials is an effective strategy for constructing hollow and yolk-shell NPs. Herein, we reported the facile synthesis of Cu@SiO₂ yolk-shell NPs by converting the silica-encapsulated Cu₂O nanoparticle aggregates (NPAs) via a disproportionation reaction. This method was extremely simple and scalable. In addition, all of the reactions were conducted in air and water solutions that are easily scalable to a mass production scale.

1. Introduction

Copper, which is an inexpensive and versatile material, has been used since ancient times in various fields due to its excellent mechanical, electrical and thermal characteristics. In the past few decades, Cu-based nanomaterials have been considered a promising catalyst for the hydrogenolysis of C-O bonds,[1-3] the epoxidation of propylene,[4] and the low-temperature water-gas shift reaction[5] due to its high selectivity, activity and low cost. However, the use and synthesis of Cu nanomaterials is challenging due to the ease of oxidation and the difficult synthesis due to the relatively low reduction potential of Cu^{2+}.[6]

Previously, we reported the crystal-to-crystal conversion of Cu₂O NPAs to Cu crystals.[7] The Cu₂O NPAs, which are composed of packed ~5 nm Cu₂O primary NPs, was reduced to metallic Cu by ascorbic acid in air. However, the conversion was not controllable due to very inhomogeneous Cu crystals. Encapsulation of Cu₂O NPAs using a SiO₂ shell efficiently confines the reaction in a sub-micron reactor. Therefore, we can easily control the conversion reaction. Only the Cu₂O NPAs inside the well-controlled SiO₂ shell are transformed to uniform Cu crystals. In addition, the resulting structure is expected to be a so-called yolk-shell structure in which movable Cu crystals are inside the SiO₂ shell.

This interesting nanostructure has attracted considerable attention due to its fundamental scientific significance and various technological applications, such as catalysis,[8-11] drug delivery,[12] and energy storage.[13] In general, yolk-shell NPs were created by selectively scarifying the core/shell layer[14-16] or converting the core materials via a disproportionation reaction,[17] galvanic reaction[18] or Kirkendall effect.[19] Based on these technologies, various yolk-shell NPs have been synthesized.[20-22] However, most of the studies on preparing yolk-shell NPs are focused on physicochemically stable materials, such as Au, Ag, and Pt as the core and SiO₂, TiO₂, and Fe₂O₃ as the shell. A few synthetic procedures for the preparation of yolk-shell NPs with a Cu core have been published. For example, Hah et al. reported the synthesis of Cu@SiO₂ yolk-shell NPs by introducing Cu salt into the cavity of hollow SiO₂ NPs followed by chemical reduction.[23] However, a large quantity of Cu NPs was formed outside the shell after the reduction of Cu salts, which results in complicated purification of the yolk-shell NPs. Su et al. also synthesized a Cu@SiO₂ yolk-shell composite by reducing of Cu₂O@SiO₂ core-shell composites.[17] However, the encapsulation and reduction were difficult to control, and many broken NPs and substantial SiO₂ aggregates on the shell surface were observed in the final Cu/SiO₂ composite.

In this study, we developed a facile synthetic method for Cu@SiO₂ yolk-shell NPs with a well-defined structure. This method was simple and scalable, and all of the reactions were conducted in air and water solutions, which are easily scalable to a mass production scale.

2. Experimental Section

2.1 Materials and Methods

Copper(II) acetate monohydrate (Cu(Ac)₂•H₂O), polyvinylpyrrolidone (PVP, Mw = 10,000 g/mol), polyacrylamide (PAM, Mw = 1,500 g/mol), L(+)-ascorbic acid, tetraethyl orthosilicate (TEOS), a NaOH aqueous solution (0.1 M), ammonia hydroxide (NH₃•H₂O, 28~30% NH₃ basis), and a H₂SO₄ solution (0.25 M) were purchased from Sigma–Aldrich. Ethanol and acetone were supplied by Samchun Chemical. All of the chemical reagents were used without further purification. The crystal NPs of the samples were characterized by a Micro-Area X-ray diffractometer (DMAX-2000(18 kW)) with Cu Kα radiation (λ=1.5418 Å). The

morphology and size of the samples were characterized using a Hitachi Model S-4800 field-emission scanning electron microscopy (FESEM) system at an acceleration voltage of 10 kV and a JEOL 3000F transmission electron microscope (TEM) operated at 300 kV. The infrared (IR) spectra were recorded on a Shimadzu IRAffinity-1 FT-IR spectrometer using KBr pellets. The compositions of the nanoNPs were determined using EDX analysis (equipped with FESEM).

2.2 Synthesis of the Cu_2O NPAs.

The spherical Cu_2O NPAs were synthesized according to a previously reported procedure except the PAM surfactant was replaced with PVP.[24] In a typical procedure, $Cu(Ac)_2 \cdot H_2O$ (18 g), PVP-10,000 (108 g) and H_2O (1800 ml) were added to a 2 L beaker containing a magnetic stir bar at room temperature. After the dissolution of $Cu(Ac)_2 \cdot H_2O$ and PVP, ascorbic acid (18 g) was quickly added to the mixture solution with a stirring rate of 80 rpm and allowed to react for 1 minute. After the reaction, the suspension was centrifuged (2500 rpm, 3 min) and washed twice with distilled water and ethanol. The product (6.2 g) was obtained after drying in vacuum at room temperature with a nearly 100 % yield.

2.3 Encapsulation of Cu_2O NPAs using the sol-gel method.

The $Cu_2O@SiO_2$ NPs were obtained via a sol-gel process consisting of hydrolysis and condensation of TEOS in ethanol/H_2O using NaOH as the catalyst. Specifically, the Cu_2O NPAs (0.75 g) were re-dispersed in a solution (1455 mL, 18 wt% water in ethanol) using ultra sonication for 2~3 min. After stirring for 15 min, the as-prepared TEOS solution in ethanol (30 mL, 6 wt%) was added to the solution and stirred for an additional 15 min. Then, the NaOH aqueous solution (15 mL, 0.1 M) was introduced dropwise in 5 min to the solution with a stirring rate of 600 rpm at room temperature. After 24 h, the $Cu_2O@SiO_2$ NPs were collected by centrifugation (2500 rpm, 3 min) and washed twice with ethanol/water (2:1 vol/vol). The product was obtained by drying in vacuum at room temperature.

2.4 Reaction of the $Cu_2O@SiO_2$ NPs.

The $Cu_2O@SiO_2$ NPs (0.1 g) were dispersed in water (20 mL) using sonication for 2 minutes, and then, H_2SO_4 (100 mL, 0.25 M) or ascorbic acid (0.1 g) was added to the dispersion solution for the specified reaction time at room temperature. The products were collected by centrifugation (2500 rpm, 3 min) and washed 3 times with H_2O.

3. Results and discussion

The structural transformation process is shown in Scheme 1. First, the Cu_2O NPAs were encapsulated in silica via a modified Stöber method. Next, the $Cu@SiO_2$ yolk-shell NPs were created by converting the encapsulated Cu_2O NPAs to Cu crystals via a disproportionation reaction with H_2SO_4.
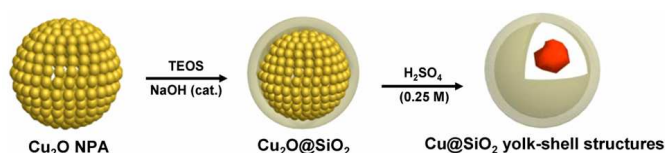
Scheme 1. Procedure for the synthesis of $Cu@SiO_2$ yolk-shell NPs.

The Cu_2O NPAs were produced by reduction of $Cu(Ac)_2$ with ascorbic acid and a PVP surfactant at room temperature for less than a minute in air. The FESEM image (Figure 1a) indicated that the synthesized Cu_2O NPAs are highly spherical with a diameter of 400~600 nm, and the size of the Cu_2O NPAs were controlled by varying the PVP concentration used (Figure S1). The prepared Cu_2O NPAs were composed of packed ~5 nm primary NPs (Figure S2). In addition, this characteristic secondary aggregation structure was similar to the result for Cu_2O NPAs with PAM surfactant in our previous paper.[24]
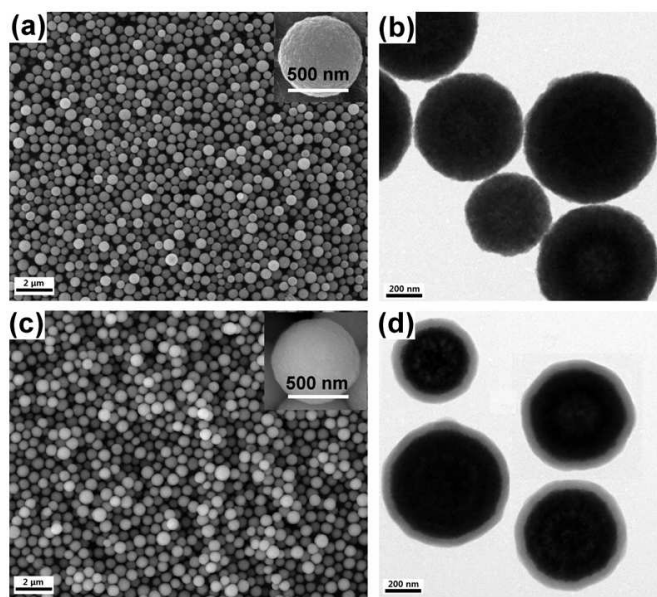
Figure 1. SEM images of Cu_2O NPAs (a) and silica-encapsulated Cu_2O NPAs (c) (insets: the corresponding SEM images of a single NP). (b) and (d) are the relevant TEM images.

Then, the Cu_2O NPAs were encapsulated in silica via a sol-gel reaction using TEOS as a silica source and NaOH as a catalyst. Based on the SEM image, no aggregation of the Cu_2O NPAs and secondary nucleation of SiO_2 NPs were observed under the chosen conditions (Figure 1c). Based on the TEM image (Figure 1d), the shell has a uniform thickness of approximately 50 nm. No morphological and structural changes of the core were observed compared to that prior to encapsulation (Figure 1b), indicating the Cu_2O NPAs were sufficiently stable during the growth of the silica shell. The thickness of the silica shell increased from 19 nm to 60 nm according to the reaction time, and the encapsulation reaction was nearly complete within 8 h (Figure S3).

To further confirm the successful SiO_2 encapsulation on the surfaces of Cu_2O NPAs, IR measurements were performed. For the Cu_2O NPAs, the IR absorption peaks at 1646 cm^{-1} are the characteristic absorptions of PVP and the peak at 631 cm^{-1} corresponds to the Cu-O stretching vibration (Figure 2a-1). After SiO_2 encapsulation, the characteristic vibration of the Si-O-Si bonds at 1081 cm^{-1}, 804 cm^{-1} and 461 cm^{-1} and the bending vibration of Si-OH bonds at 960 cm-1 were observed. The peak at 1203 cm^{-1} was due to the deformed network of SiO_2. The deformation of the SiO_2 network may be due to the formation of Cu-O-Si bonds at the interface between the Cu_2O NPAs core and the SiO_2 shell, which altered the bond strain of Si-O-Si leading to an increase in the disorder of the SiO_2

network. This result is in agreement with a previous study were the Cu-O-Si bonds changed the bond strain of Si-O-Si.[17] The formation of Cu-O-Si bonds may facilitate the uniform encapsulation of SiO_2 around the entire surface of the Cu_2O NPAs. In addition, the Si element was detected on the surface of the encapsulated NPs in the energy-dispersive X-ray (EDX) spectrum (Figure S4), indicating the presence of SiO_2 in the resulting products. The composition of the core remains unchanged during the silica encapsulation according to the X-ray diffraction (XRD) patterns of the Cu_2O NPAs and the $Cu_2O@SiO_2$ NPs (Figures 2b-1 and 2b-2). The SiO_2 amorphous peak in the $20°$ to $25°$ range cannot be observed even with a shell thickness of 60 nm due to the intense Cu_2O peaks.
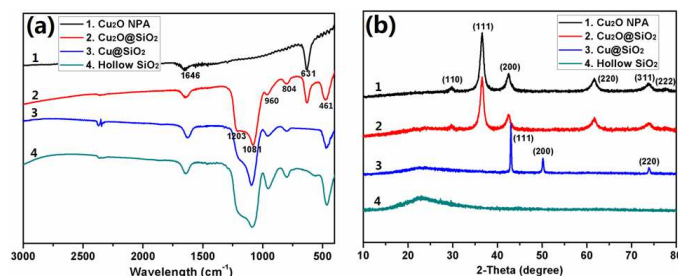
Figure 2. IR spectra (a) and XRD patterns (b) of the Cu_2O NPAs (1), $Cu_2O@SiO_2$ (2), $Cu@SiO_2$ yolk-shell NPs (3), and hollow SiO_2 NPs (4).

The successful encapsulation of Cu_2O NPAs with SiO_2 was due to the appropriate selection of surfactant and catalyst for the Stöber method. In general, PVP is used as a surfactant to assist in encapsulating colloids with silica or other oxide shells due to its amphiphilic and non-ionic characteristics.[25-27] Therefore, in this study, the PVP surfactant was substituted for PAM to synthesize the Cu_2O NPAs. It is important to note that it is difficult to encapsulate silica in the Cu_2O NPAs with the PAM surfactant due to the poor chemical affinity between TEOS and PAM as well as the poor solubility of the PAM surfactant in ethanol (Figures S5 and S6). For the catalyst, because $NH_3 \cdot H_2O$ can quickly etch the Cu_2O NPAs core via facile formation of coordination complexes (Figure S7),[28] NaOH was chosen for catalyzing the encapsulation of Cu_2O NPAs.[29-31] The TEM image (Figure S8) and XRD analysis (Figures 2b-1 and 2b-2) also revealed that the etching of the Cu_2O NPAs by NaOH can be ignored.

Cuprous compounds can go through a disproportionation reaction to form Cu metal and Cu^{2+} ion under acidic conditions.[32,33] Therefore, the encapsulated Cu_2O NPAs were further used as starting material to study the spatially confined conversion of Cu_2O NPAs to Cu crystals.

$Cu@SiO_2$ yolk-shell NPs were obtained when the $Cu_2O@SiO_2$ NPs were added to H_2SO_4 with a high concentration (0.25 M). The solution became blue-green, and the weight loss of the $Cu_2O@SiO_2$ NPs was approximately 42%, which is similar to the theoretical weight loss (39%) of the product in the disproportionation reaction (see the Supporting Information), indicating that the Cu^{2+} ions generated from the disproportionation diffused to the solution through the SiO_2 shell. The TEM image shows that the yolk-shell structure of the Cu core and SiO_2 shell due to the clear contrast difference between the core and the shell (Figure 3a). The EDX spectrum shows strong Cu peaks, indicating the conversion of Cu_2O to Cu metal inside the SiO_2 reactor (Figure S9). From the XRD pattern, the intrinsic diffraction peaks of Cu (43.3°, 50.5° and

74.2°) and the amorphous peak of SiO_2 in the range of 20° to 25° were observed (Figure 2b-3). No other peaks were detected in the XRD pattern for the $Cu@SiO_2$ yolk-shell NPs, implying that the high purity of the Cu crystal was produced by the simple acid treatment process. The disappearance of the Cu-O vibration peak at 631 cm^{-1} in the IR spectrum also demonstrated that all of the Cu_2O was converted into Cu metal (Figure 2a-3). The SEM image revealed that nearly all of the NPs remained intact without aggregation after the H_2SO_4 treatment (Figures 3b and S10). The $Cu_2O@SiO_2$ NPs with a shell thickness of 60 nm were sufficiently robust to withstand the osmotic pressure associated with mass diffusion. When the $Cu_2O@SiO_2$ NPs with a thinner shell layer of 34 nm were treated with 0.25 M H_2SO_4, partial $Cu_2O@SiO_2$ NPs were broken and various dispersed Cu NPs were observed outside of the NPs (Figure S11).
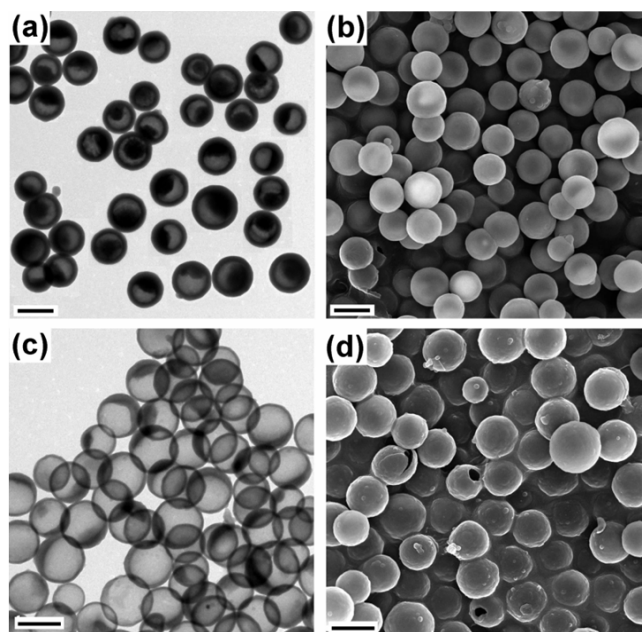
Figure 3. TEM images of $Cu@SiO_2$ yolk-shell NPs with a shell thickness of 60 nm (a) and hollow SiO_2 NPs (shell thickness of 34 nm) (c). (b) and (d) are the relevant SEM images. All of the scale bars represent 500 nm.

$Cu@SiO_2$ yolk-shell NPs can also be created using other acids, such as HCl and ascorbic acid (Figures S12 and S13). However, the obtained products were a mixture of $Cu@SiO_2$ yolk-shell NPs and hollow SiO_2 NPs. In addition, the proportion of $Cu@SiO_2$ yolk-shell NPs related to hollow NPs varied with the concentration of the acids used and the $Cu@SiO_2$ yolk-shell NPs were difficult to separate by fractional centrifugation. For example, when the $Cu_2O@SiO_2$ NPs were treated with a low concentration of HCl (0.1 M), the majority of the products were hollow SiO_2 NPs with a few $Cu@SiO_2$ yolk-shell NPs (Figure S12). For 20 wt% ascorbic acid, the products consisted of a mixture of $Cu@SiO_2$ yolk-shell NPs and hollow SiO_2 NPs. In addition, many irregular Cu microparticles were observed outside of the yolk-shell and hollow SiO_2 NPs (Figure S13). This reason can be ascribed to the reduction ability of ascorbic acid and the absence of the protective surfactants in the aqueous solution.

The formation of $Cu@SiO_2$ yolk-shell NPs was due to the disproportionation reaction of Cu^+ inside the SiO_2 sub-micron

reactor. The silica shell, created by the Stöber method, is porous with a pore size about 3.0 Å.[34,35] The size is sufficiently large to allow free diffusion of H^+, Cu^+ (diameter: 1.5 Å), and Cu^{2+} ions across the silica layer.[36] According to this fact, the H^+ ions from the acid solution diffuse into the interior of the SiO_2 reactor and dissolve in the Cu_2O NPAs core. Then, the free Cu^+ ions undergo a disproportionation reaction, which lead to the formation of Cu NPs within the SiO_2 shell resulting in the formation of $Cu@SiO_2$ yolk-shell NPs (Figure 4). The Cu^+ ions generated from H^+ dissolution of the Cu_2O NPAs core also diffused out of the reactor. Therefore, when the concentration of H^+ ions in the aqueous solution was low, the rate of formation of the Cu^+ ions was slower than the diffusion rate of the Cu^+ ions, and the disproportionation reaction was restrained. Therefore, a relatively high concentration of H^+ facilitates the formation of $Cu@SiO_2$ yolk-shell NPs, and the low concentration of H^+ tends to result in the formation of hollow SiO_2 NPs.
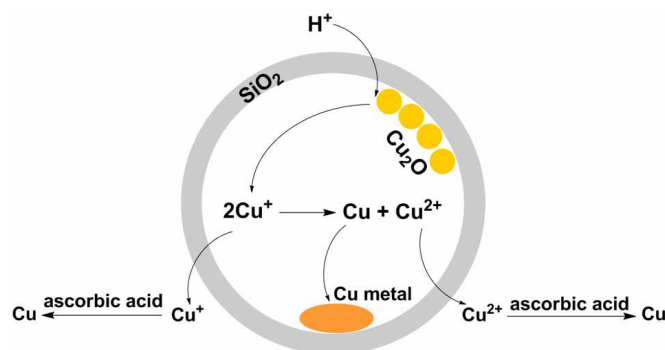
Figure 4. Schematic illustration of the conversion of Cu_2O NPAs into Cu metal via an acid treatment.

Hollow SiO_2 NPs were obtained in a high yield without $Cu@SiO_2$ yolk-shell NPs when the $Cu_2O@SiO_2$ NPs were reacted with diluted ascorbic acid (0.5 wt%). The obtained hollow SiO_2 NPs can be easily separated from the Cu micro-particles in a colloid solution using fractional centrifugation (Figure S14). The TEM (Figure 3c) and SEM (Figure 3d) images revealed that the hollow SiO_2 NPs with a shell thickness of 34 nm were sufficiently robust to withstand the osmotic pressure associated with mass diffusion. The high purity of the hollow SiO_2 NPs was confirmed by the IR spectrum (Figure 2a-4), XRD pattern (Figure 2b-4), and EDX (Figure S15).

4. Conclusions

In summary, we developed a simple and effective method for the preparation of $Cu@SiO_2$ yolk-shell NPs via a disproportionation reaction of the Cu_2O NPAs inside the SiO_2 sub-micron reactor. In comparison to previous methods for preparing Cu based yolk-shell NPs, our method has the following advantages: (1) The Cu_2O NPAs template can be easily synthesized on a large scale with nearly 100% yield at room temperature in air. (2) The sol-gel process, which provides a controllable shell thickness, can be conducted directly on the surface of the template without additional surface-modifications. (3) The template can be easily removed or transformed into other species due to the small primary Cu_2O NPs with a high surface area and the assembled secondary structure. (4) All of the reactions during the structural

transformation process can be conducted under ambient and aqueous conditions via a simple procedure. More importantly, the oxidation of the Cu core was significantly reduced due to the Cu NPs, which were encapsulated with a well-controlled SiO_2 shell. No oxidation of the Cu core was observed after storing the $Cu@SiO_2$ yolk-shell NPs for 6 months in air at room temperature. Based on these results, we believe that our $Cu@SiO_2$ yolk-shell NPs may have many potential applications. The application of the $Cu@SiO_2$ yolk-shell NPs as a catalyst is currently being investigated.

Notes and references

Department of Chemistry, Kongju National University, Chungnam, 314-701, Korea.
E-mail: sangho1130@kongju.ac.kr, piaolh@kongju.ac.kr.

1   H. Yue, Y. Zhao, S. Zhao, B. Wang, X. Ma and J. Gong, *Nat. Commun.*, 2013, **4**, 2339.
2   C. W. Li, J. Ciston and M. W. Kanan, *Nature*, 2014, **508**, 504-507.
3   K. Manthiram, B. J. Beberwyck and A. P. Alivisatos, *J. Am. Chem. Soc.*, 2014, **136**, 13319-13325.
4   A. Marimuthu, J. Zhang and S. Linic, *Science*, 2013, **339**, 1590-1593.
5   C. S. Chen, J. H. Lin, J. H. You and C. R. Chen, *J. Am. Chem. Soc.*, 2006, **128**, 15950-15951.
6   H. Guo, Y. Chen, M. B. Cortie, X. Liu, Q. Xie, X. Wang and D.-L. Peng, *J. Phys. Chem. C*, 2014, **118**, 9801-9808.
7   W.-r. Lee, Y. S. Lim, S. Kim, J. Jung, Y.-K. Han, S. Yoon, L. Piao and S.-H. Kim, *J. Mater. Chem.*, 2011, **21**, 6928-6933.
8   I. Lee, J. B. Joo, Y. Yin and F. Zaera, *Angew. Chem. Int. Ed.*, 2011, **50**, 10208-10211.
9   C.-H. Kuo, Y. Tang, L.-Y. Chou, B. T. Sneed, C. N. Brodsky, Z. Zhao and C.-K. Tsung, *J. Am. Chem. Soc.*, 2012, **134**, 14345-14348.
10 X. Huang, C. Guo, J. Zuo, N. Zheng and G. D. Stucky, *Small*, 2009, **5**, 361-365.
11 W. Li, Y. Deng, Z. Wu, X. Qian, J. Yang, Y. Wang, D. Gu, F. Zhang, B. Tu and D. Zhao, *J. Am. Chem. Soc.*, 2011, **133**, 15830-15833.
12 J. Gao, G. Liang, B. Zhang, Y. Kuang, X. Zhang and B. Xu, *J. Am. Chem. Soc.*, 2007, **129**, 1428-1433.
13 Z. Wei Seh, W. Li, J. J. Cha, G. Zheng, Y. Yang, M. T. McDowell, P.-C. Hsu and Y. Cui, *Nat. Commun.*, 2013, **4**, 1331.
14 J. Lee, J. C. Park and H. Song, *Adv. Mater.*, 2008, **20**, 1523-1528.
15 J. Lian, Y. Xu, M. Lin and Y. Chan, *J. Am. Chem. Soc.*, 2012, **134**, 8754-8757.
16 Y. J. Wong, L. Zhu, W. S. Teo, Y. W. Tan, Y. Yang, C. Wang and H. Chen, *J. Am. Chem. Soc.*, 2011, **133**, 11422-11425.
17 S. Xiaodan, Z. Jingzhe, Z. Xu, G. Yupeng, Z. Yanchao and W. Zichen, *Nanotechnology*, 2008, **19**, 365610.
18 Y. Sun, B. Wiley, Z.-Y. Li and Y. Xia, *J. Am. Chem. Soc.*, 2004, **126**, 9399-9406.
19 Y. Yin, R. M. Rioux, C. K. Erdonmez, S. Hughes, G. A. Somorjai and A. P. Alivisatos, *Science*, 2004, **304**, 711-714.
20 H. Liu, J. Qu, Y. Chen, J. Li, F. Ye, J. Y. Lee and J. Yang, *J. Am. Chem. Soc.*, 2012, **134**, 11602-11610.
21 M. Priebe and K. M. Fromm, *Chem. Eur. J.* 2014, **20**, 1-22.
22 J. Liu, S. Z. Qiao, J. S. Chen, X. W. Lou, X. Xing and G. Q. Lu, *Chem. Commun.*, 2011, **47**, 12578-12591.
23 H. J. Hah, J. I. Um, S. H. Han and S. M. Koo, *Chem. Commun.*, 2004, 1012-1013.

24   W.-r. Lee, L. Piao, C.-H. Park, Y. S. Lim, Y. R. Do, S. Yoon and S.-H. Kim, *J. Colloid Interface Sci.*, 2010, **342**, 198-201.

25   C. Graf, D. L. J. Vossen, A. Imhof and A. van Blaaderen, *Langmuir*, 2003, **19**, 6693-6700.

26   H. Sun, J. He, J. Wang, S.-Y. Zhang, C. Liu, T. Sritharan, S. Mhaisalkar, M.-Y. Han, D. Wang and H. Chen, *J. Am. Chem. Soc.*, 2013, **135**, 9099-9110.

27   G. Lu, S. Li, Z. Guo, O. K. Farha, B. G. Hauser, X. Qi, Y. Wang, X. Wang, S. Han, X. Liu, J. S. DuChene, H. Zhang, Q. Zhang, X. Chen, J. Ma, S. C. J. Loo, W. D. Wei, Y. Yang, J. T. Hupp and F. Huo, *Nat. Chem.*, 2012, **4**, 310-316.

28   H. Yang, Y. Min, Y. Kim and U. Jeong, *Colloids Surf., A*, 2013, **420**, 30-36.

29   J. Nai, Y. Tian, X. Guan and L. Guo, *J. Am. Chem. Soc.*, 2013, **135**, 16082-16091.

30   Y. Kobayashi, H. Inose, T. Nakagawa, K. Gonda, M. Takeda, N. Ohuchi and A. Kasuya, *J. Colloid Interface Sci.*, 2011, **358**, 329-333.

31   B. P. Khanal, A. Pandey, L. Li, Q. Lin, W. K. Bae, H. Luo, V. I. Klimov and J. M. Pietryga, *ACS Nano*, 2012, **6**, 3832-3840.

32   J. Malyszko and M. Kaczor, *J. Chem. Educ.*, 2003, **80**, 1048-1050.

33   Q. Zhang, P. Wilson, Z. Li, R. McHale, J. Godfrey, A. Anastasaki, C. Waldron and D. M. Haddleton, *J. Am. Chem. Soc.*, 2013, **135**, 7355-7363.

34   A. Walcarius, C. Despas and J. Bessière, *Microporous Mesoporous Mater.*, 1998, **23**, 309-313.

35   K. P. Velikov and A. van Blaaderen, *Langmuir*, 2001, **17**, 4779-4786.

36   R. D. Shannon, *Acta Cryst. A*, 1976, **32**, 751-767.

Nanoscale Accepted Manuscript